

## Third-order nonlinear optical response and ultrafast dynamics of tetraoxa[22]porphyrin(2.1.2.1)s<sup>†</sup>

Krishnandu Makhal,<sup>b</sup> Shafali Arora,<sup>a</sup> Paramjit Kaur,<sup>a</sup> Debabrata Goswami<sup>b,\*</sup> and Kamaljit Singh<sup>a,\*1</sup>

<sup>a</sup>Department of Chemistry, UGC Centre of Advance Study-II, Guru Nanak Dev University, Amritsar- 143005, India

<sup>b</sup>Department of Chemistry, Indian Institute of Technology, Kanpur -208016, India

\*e-mail: [kamaljit.chem@gndu.ac.in](mailto:kamaljit.chem@gndu.ac.in); [dgoswami@iitk.ac.in](mailto:dgoswami@iitk.ac.in)

S. No.	Content	Page number
1.	Experimental set up for z-scan measurements (Fig. S1) and the related theory.	S1-S3
2.	Copies of <sup>1</sup> H NMR, <sup>13</sup> C NMR and HR mass Spectra of <b>5</b> and intermediates (Fig S2-S12).	S4-S11
3.	The steady state absorption spectra (blue line) of compounds 4-6 recorded in DCM along with the theoretical vertical excitation energies (red bar) obtained from TD-DFT calculations carried out at the B3LYP/6-311G basis set (Fig. S13).	S12
4.	Calculation of NICS of <b>5</b> (Fig. S14-16).	S13-S15
5.	Molecular structures (optimized at Gaussian 09 B3LYP/6-311G (d)) and their molecular dimensions (Fig. S17).	S16
6.	Energy minimized structure of <b>5</b> by DFT method at B3LYP/6-311G(d) level using the Gaussian09 program (Top and side view) (Fig. S18).	S17
7.	Fluorescence lifetimes of three compounds measured through TCSPC with IRF of 80 ps (Fig. S19).	S18
8.	Selected TD-DFT ( B3LYP/6-311G (d)) calculated energies, oscillator strengths and compositions of the major electronic transitions of <b>4-6</b> (Tables S1-S3).	S19-S20
9.	Coordinates for the optimized structure <b>5</b> (Table S4).	S21-S22
10.	Selected Frontier MOs of <b>4-6</b> calculated at the B3LYP/6-311G(d) level (Fig. S20-S22).	S23-S25
11.	Average Polarizability of <b>4-6</b> using Gaussian 09 program (Table S5).	S26
12.	Energy level diagram (Fig. S23).	S27
13.	Plot of $\beta$ versus fluence $I_0$ (Fig. S24).	S28
14.	Femtosecond transient absorption spectra of <b>6</b> (Fig. S25).	S29
15.	Complete reference [17].	S30

<sup>†</sup> The first two authors contributed equally

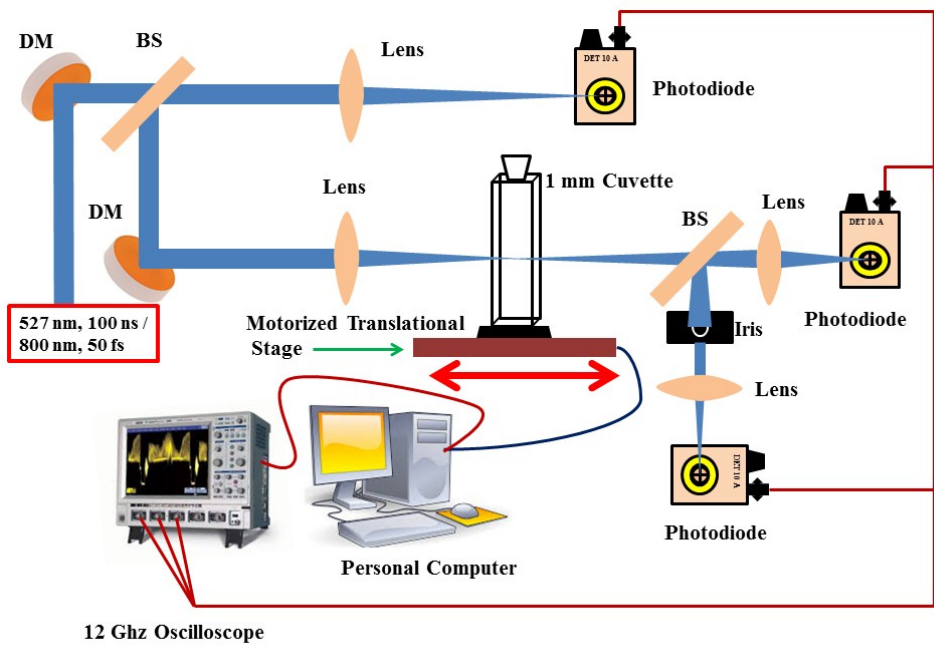


**Figure S1:** Experimental setup for Z-scan for measurements.

## Theory related to the nonlinear phenomenon used in the manuscript:

The nonlinear refraction coefficient  $\gamma$  is defined as:

$$n = n_0 + \gamma I_0 \quad (1)$$

Where  $n_0$  is the linear index of refraction,  $I_0$  is the on axis intensity at the beam waist. Similarly the nonlinear absorption coefficient is defined by

$$\alpha = \alpha_0 + \beta I_0 \quad (2)$$

Where  $\alpha_0$  is the linear absorption coefficient. Under Open aperture condition, the normalized transmittance is given by<sup>1,2</sup>

$$T(z) = 1 - \frac{q_0}{2\sqrt{2}} \quad \text{for } |q_0| < 1 \quad (3)$$

$$q_0 = \frac{\beta I_0 (1 - e^{-\alpha_0 L})}{(1 + \frac{z^2}{z_0^2}) \alpha_0} = \frac{\beta I_0 L_{eff}}{(1 + \frac{z^2}{z_0^2})} \quad (3)$$

where the free factor  $q_0$  is defined as

where  $\alpha_0$  is the linear absorption coefficient,  $L$  is the thickness of the sample,  $I_0$  is the intensity at the focus ( $z=0$ ) and  $z_0$  is the Rayleigh range. The OA Z-scan experiment determines the magnitude of nonlinear absorption coefficient  $\beta$  which is related to imaginary part of  $\chi(3)$ . The change in beam intensity after transmitting through the sample can be written as<sup>1,2</sup>

$$\frac{dI}{dz} = -\alpha_0 I - \sigma_{ex} N(t) I \quad (4)$$

Where  $z$  is the position of the sample,  $I$  is the intensity,  $N$  is the density of the molecule in the excited state and  $\alpha_0$  is the linear absorption coefficient. Number density  $N(t)$  of the molecules appears a result of nonlinear absorption process in the excited triplet state to higher triplet state as the ns pulse width ( $\tau$ ) > ISC and the intensity dependence can be expressed as<sup>3,4</sup>

$$\frac{dN}{dt} = \frac{\alpha_0 I}{hv} \quad (5)$$

where  $v$  is the frequency of laser. Combining equations 3 and 4 gives

$$\frac{dI}{dz} = -\alpha_0 I - \frac{\sigma_{ex} \alpha_0 I}{hv} \int_{-\infty}^t I(t) dt \quad (6)$$

Solving above equation for fluence and integrating over the beam gives us the normalized transmittance for OA as<sup>23</sup>

$$T = \frac{\ln(1 + \frac{q_0}{1 + x^2})}{(\frac{q_0}{1 + x^2})} \quad (7)$$

Where  $x = z/z_0$ ,  $z$  is the distance of the sample from the focus,  $z_0$  is the Rayleigh range and  $q_0$  is given by

$$q_0 = \frac{\sigma_{ex} \alpha_0 F_0 L_{eff}}{2hv} \quad (8)$$

Where  $F_0$  is the on axis fluence at the focus which is related to incident input energy over the sample. Finally the ground state absorption cross section  $\sigma_{gr}$  is calculated using the relation

$$\sigma_{gr} = \frac{\alpha_0}{N_A C} \quad (9)$$

with  $N_A$  being Avogadro's number and  $C$  is concentration used in mol/lit.

S2

Nonlinear refractive index  $\gamma$  was obtained by fitting the CA Z-scan traces obtained experimentally to the equation;

$$T = 1 + \frac{4x}{(x^2 + 9)(x^2 + 1)} \Delta\Phi - \frac{2(x^2 + 9)}{(x^2 + 9)(x^2 + 1)} \Delta\Psi \quad (10)$$

where  $\Delta\Phi = kyI_0L_{eff}$  is nonlinear phase shift due to nonlinear refraction and  $\Delta\Psi = \beta I_0 L_{eff}/2$  is nonlinear phase shift due to nonlinear absorption,  $x=z/z_0$  represents the dimensionless relative position from the beam waist,  $z_0$  being the Rayleigh range of the focused Gaussian beam,  $k$  is the wave vector,  $\gamma$  is nonlinear refractive coefficient,  $\beta$  is nonlinear absorption coefficient,  $I_0$  is the on axis power density at the beam waist and  $L_{eff}$  is the effective sample length considering linear attenuation. The real and imaginary parts of third order nonlinear susceptibility  $\chi^{(3)}$  are related to nonlinear refraction and absorption coefficients as:

$$\chi^3 = \chi_{Re}^{(3)} + \chi_{Im}^{(3)} \quad (11)$$

with  $\chi_{Re}^{(3)} = 2n_0\epsilon_0 c \gamma$  and  $\chi_{Im}^{(3)} = n_0^2 \epsilon_0 c \beta / k$

where  $c$  is the velocity of light in vacuum and  $\epsilon_0$  is permittivity of free space. Introducing  $\rho$  which is the ratio of the imaginary to real part of third order nonlinear susceptibility  $\chi^{(3)}$  as:

$$\rho = \frac{\chi_{Im}^{(3)}}{\chi_{Re}^{(3)}} = \frac{\beta}{2\kappa\gamma} \quad (12)$$

and considering equations 11 and 12 we have:

$$\Delta\Psi = \rho \Delta\Phi \quad (13)$$

Invoking equation 13 into equation 10 yields the normalized transmittance  $T$  in CA Z-scan which we have used for theoretical fitting of our CA data and is represented as:

$$T = 1 + \frac{2(-\rho x^2 + 2x - 3\rho)}{(x^2 + 9)(x^2 + 1)} \Delta\Phi \quad (14)$$

References:

- 1 F. Z. Henari, W. J. Blau, L. R. Milgrom, G. Yahioğlu, D. Philips and J. A. Lacey, *Chem. Phys. Lett.*, 1997, **267**, 229-233.
- 2 F. Z. Henari, *J. Opt. A: Pure Appl. Opt.* 2001, **3**, 188-190.
- 3 P. Poornesh, G. Umesh, P. K. Hegde, M.G. Manjunatha, K. B. Manjunatha and A. V. Adhikari, *Appl. Phys. B*, 2009, **97**, 117-124.
- 4 P. Poornesh, P. K. Hegde, G. Umesh, M.G. Manjunatha, K. B. Manjunatha and A. V. Adhikari, *Opt. Laser Tech.* 2010, **42**, 230-236.

S3

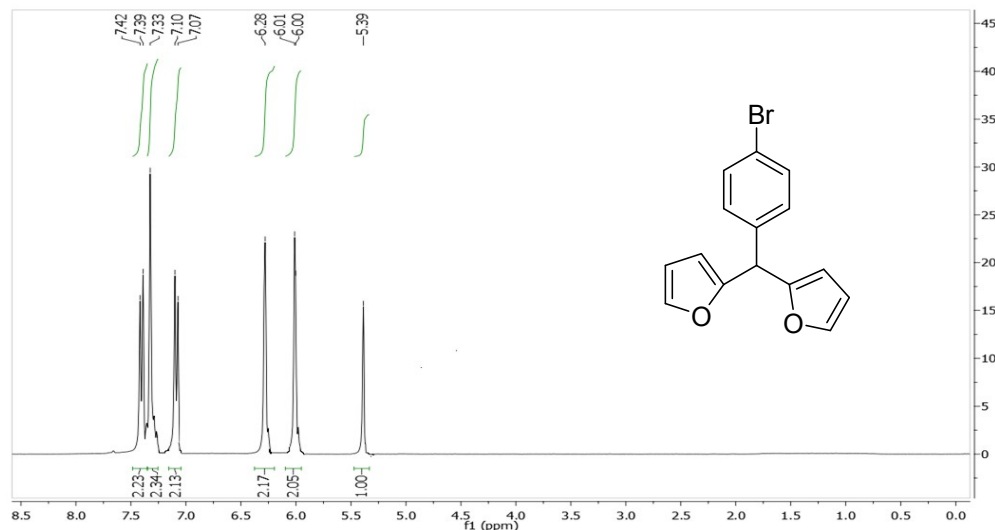


**Figure S2:** <sup>1</sup>H NMR spectrum (in  $\text{CDCl}_3$ ) of 4-Bromophenyl-di(furan-2-yl)methane.

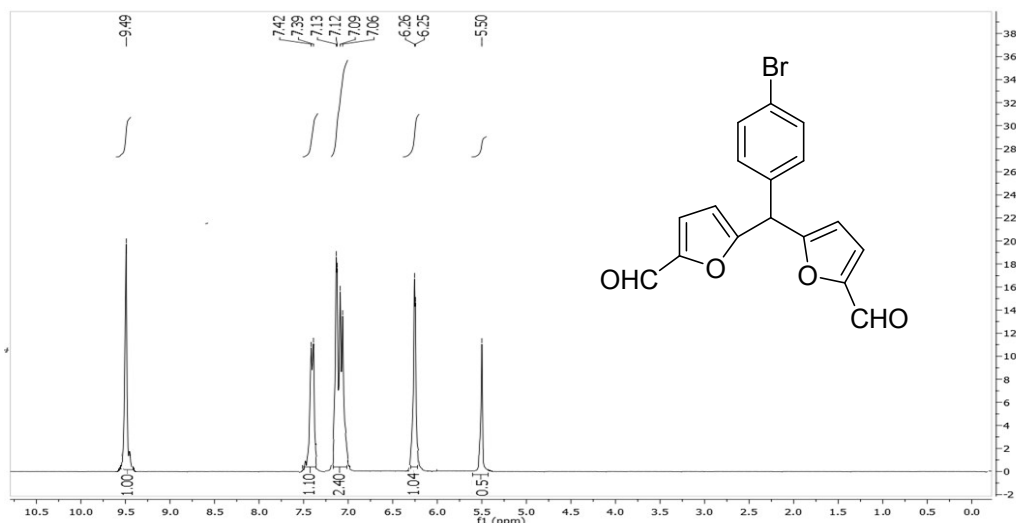


**Figure S3:** <sup>1</sup>H NMR spectrum (in  $\text{CDCl}_3$ ) of 4-Bromophenyl-di(5-formylfuran-2-yl)methane.

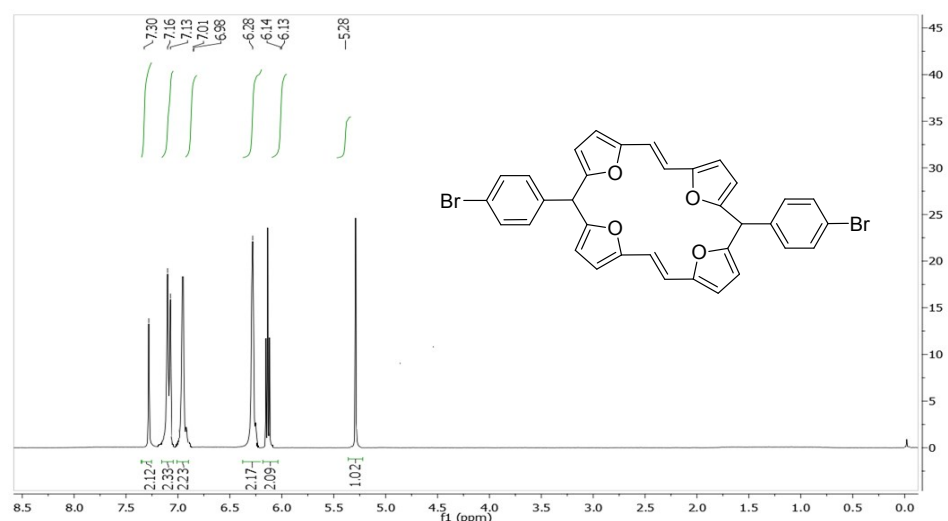


**Figure S4:** <sup>1</sup>H NMR spectrum (in CDCl<sub>3</sub>) of 5,16-Di-(4-bromo)phenyl-5,16-dihydrotetraoxa[22]porphyrin(2.1.2.1).

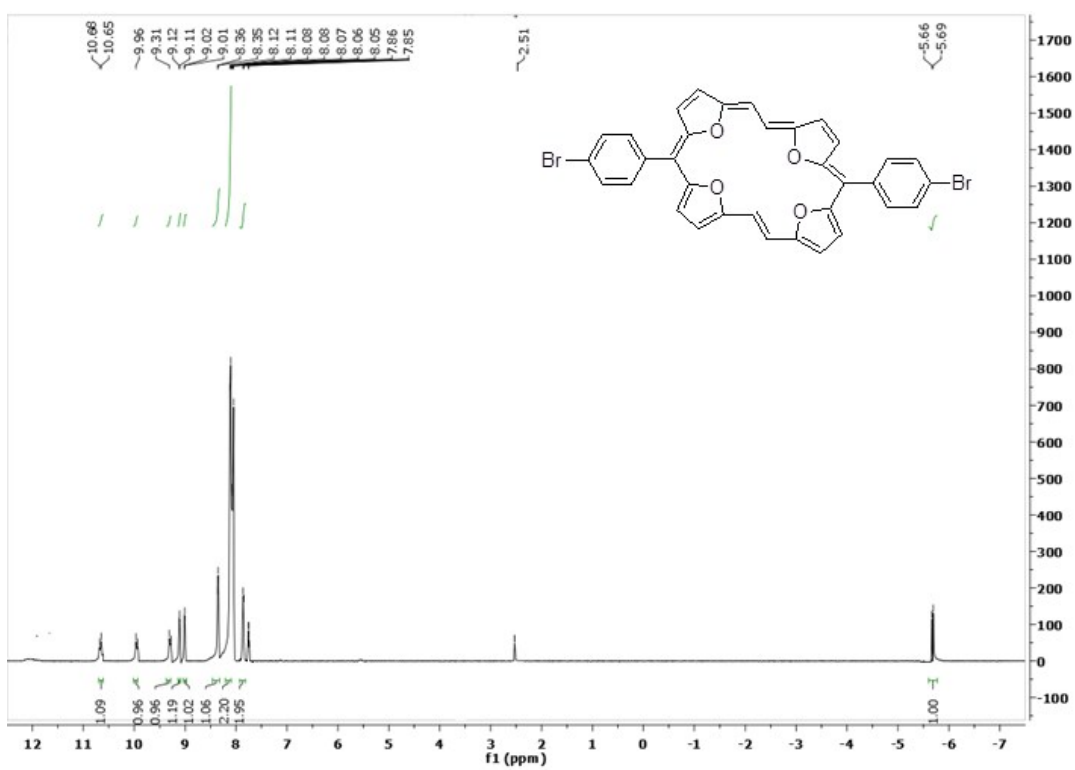


**Figure S5:** <sup>1</sup>H NMR spectrum (in DMSO-*d*<sub>6</sub>) of **5**.

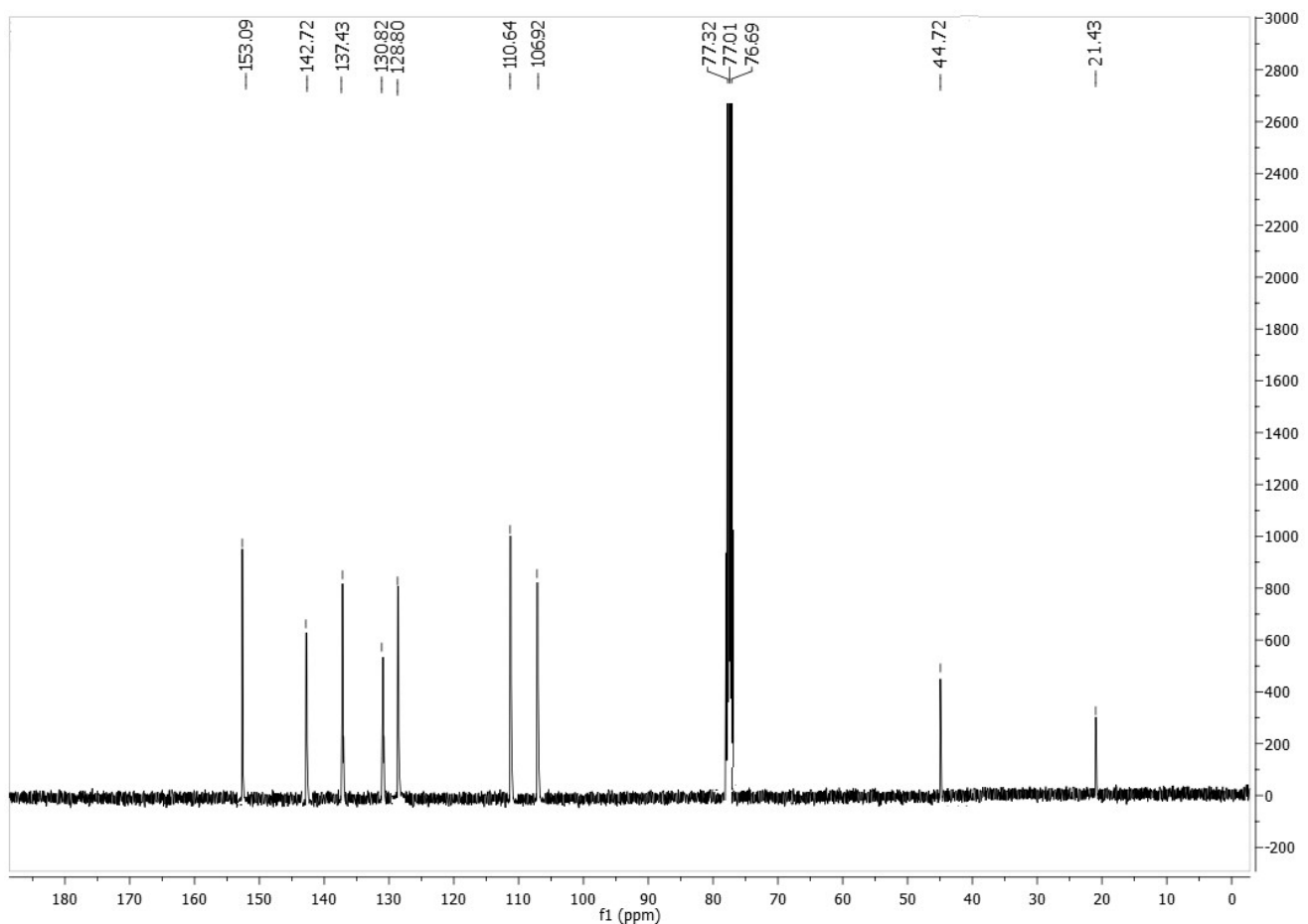


**Figure S6:**  ${}^{13}\text{C}$  NMR spectrum (in  $\text{CDCl}_3$ ) of 4-Bromophenyl-di(furan-2-yl)methane.

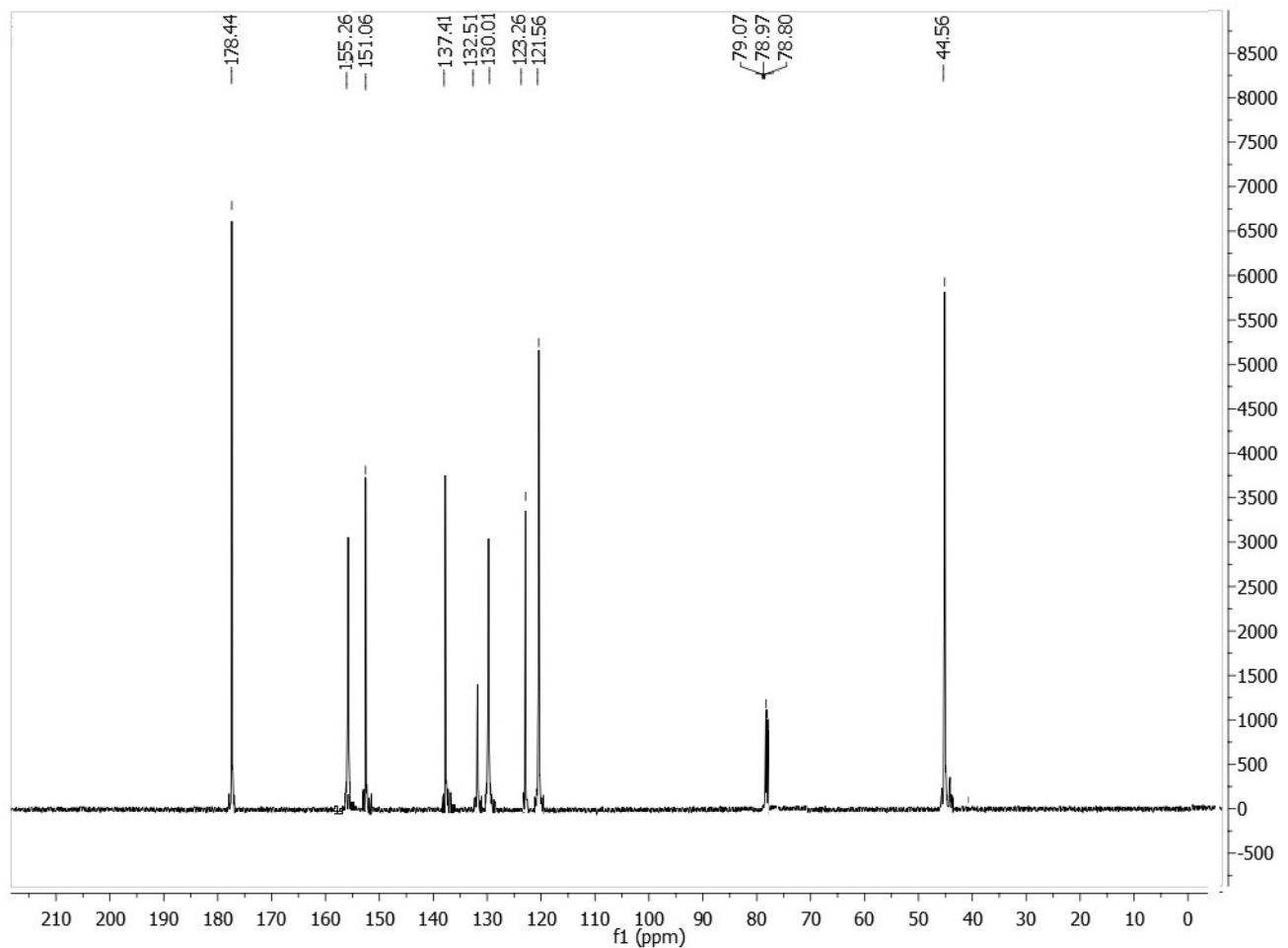


**Figure S7:**  $^{13}\text{C}$  NMR spectrum (in  $\text{CDCl}_3$ ) of 4-Bromophenyl-di(5-formylfuran-2-yl)methane.

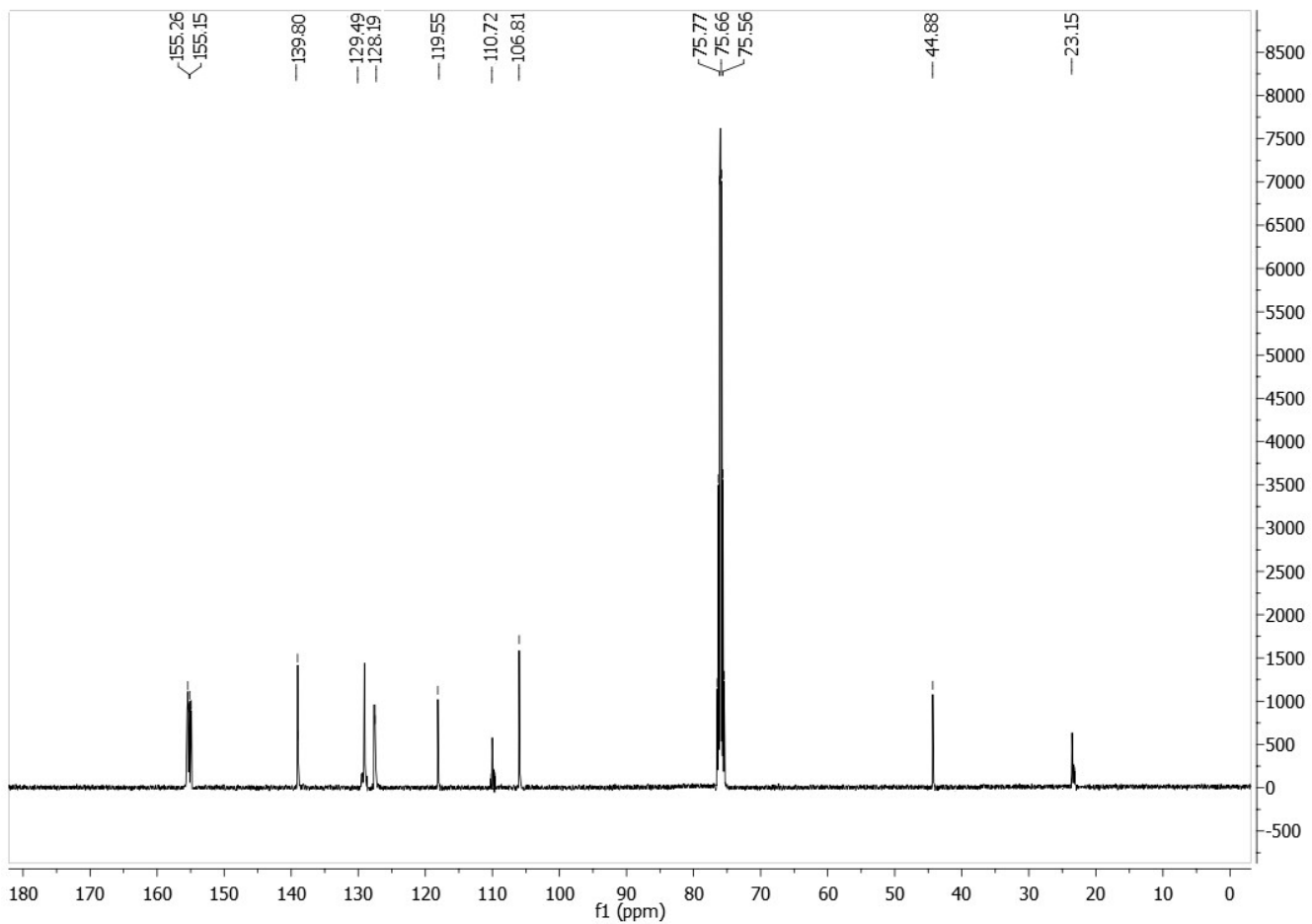


**Figure S8:**  $^{13}\text{C}$  NMR spectrum (in  $\text{CDCl}_3$ ) of 5,16-Di-(4-bromo)phenyldihydrotetraoxa[22]porphyrin(2.1.2.1).

S9

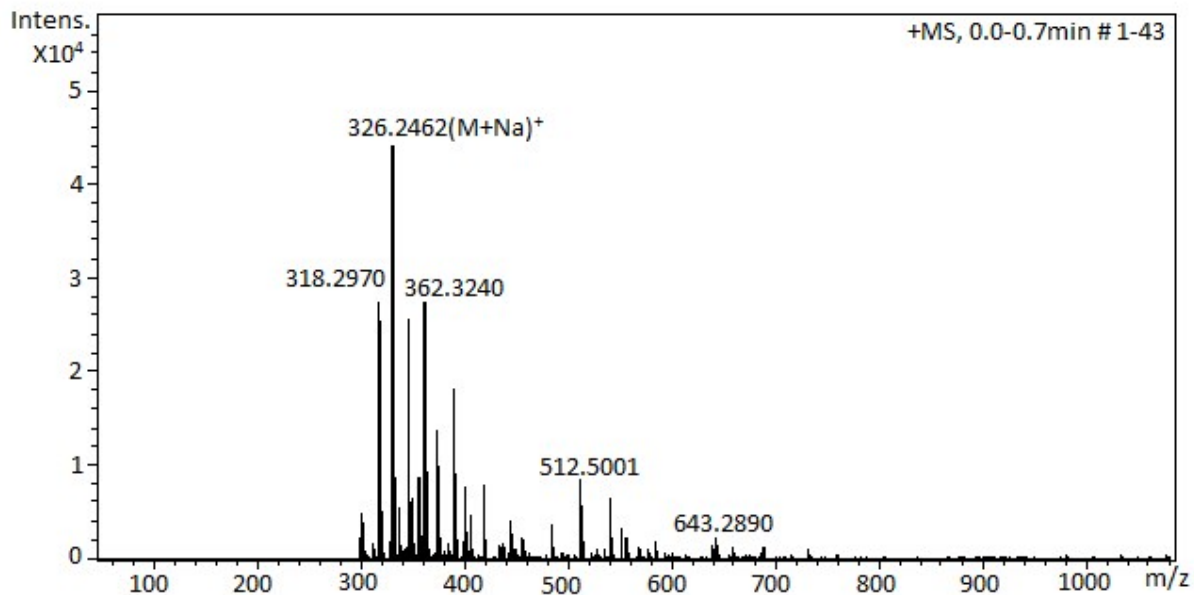


**Figure S9:** HRMS (High Resolution mass spectra) of 4-Bromophenyl-di(furan-2-yl)methane.

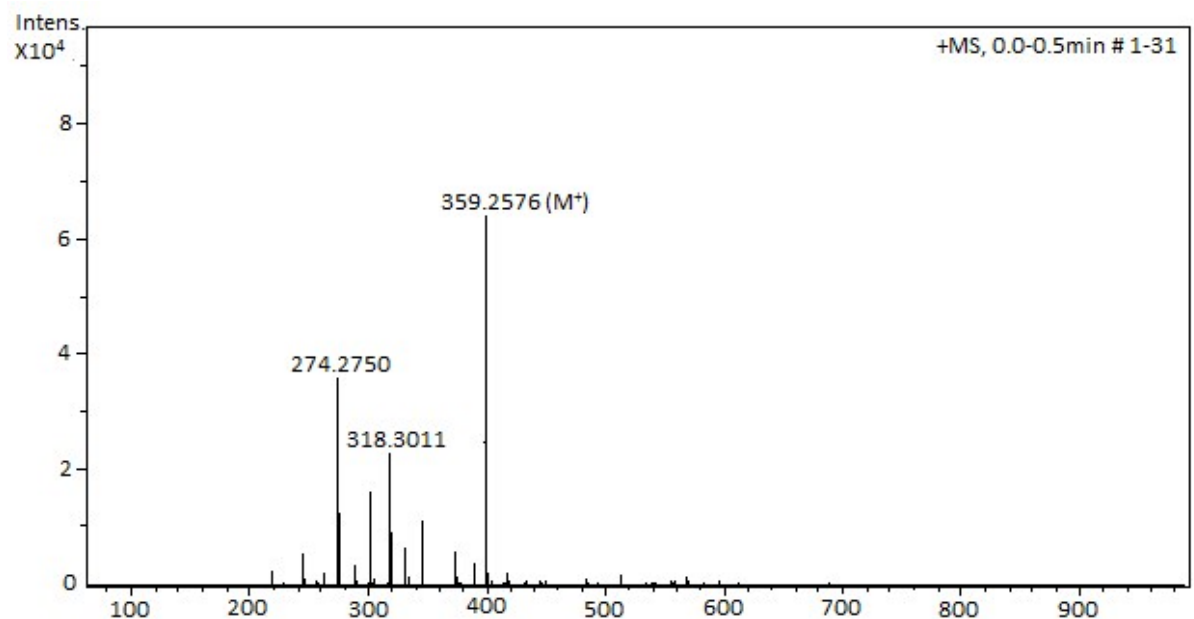


**Figure S10:** HRMS (High Resolution mass spectra) of 4-Bromophenyl-di(5-formylfuran-2-yl)methane.

S10

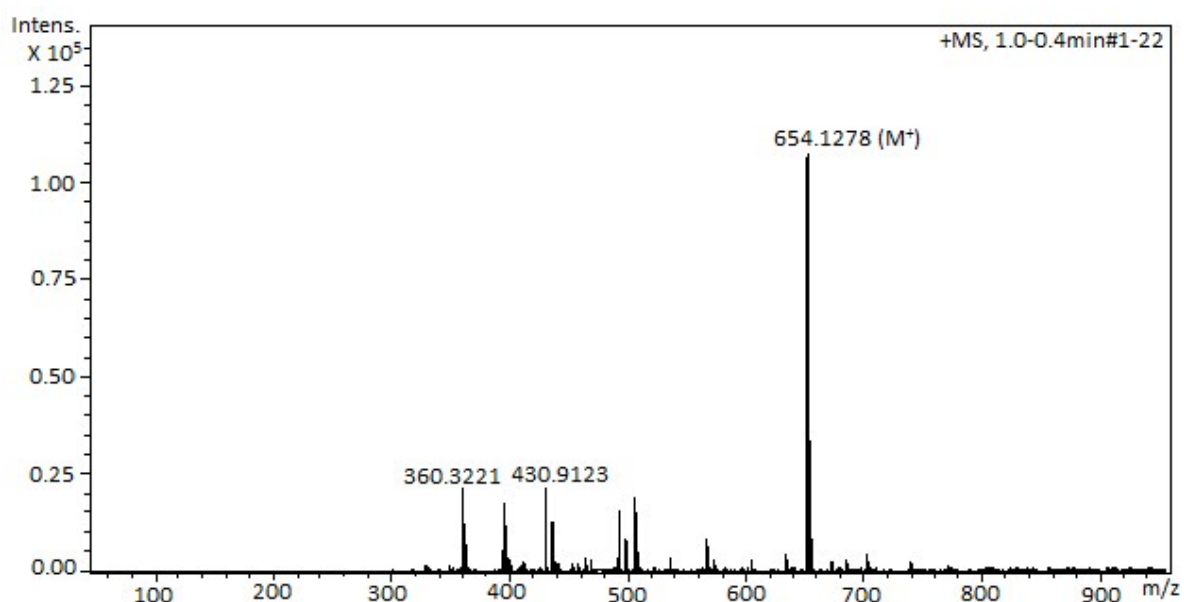


**Figure S11:** HRMS (High Resolution mass spectra) of 5,16-Di-(4-bromo)phenyldihydrotetraoxa[22]porphyrin(2.1.2.1).

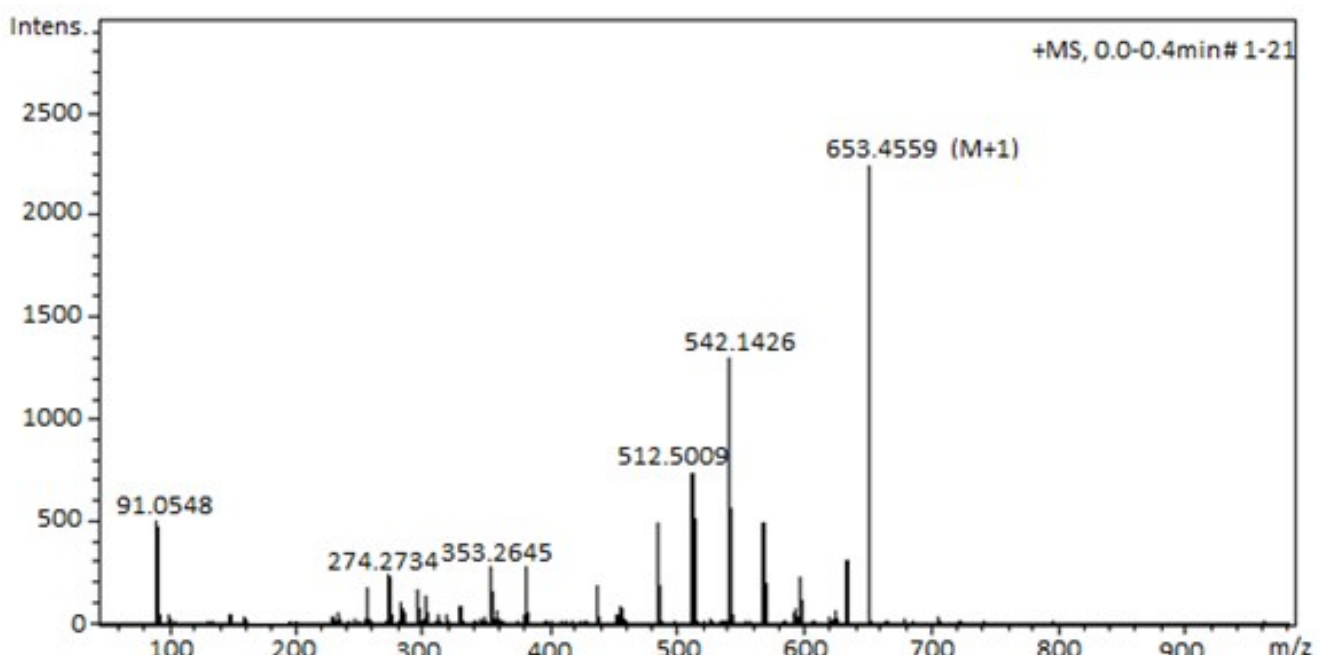


**Figure S12:** HRMS (High Resolution mass spectra) of **5**.

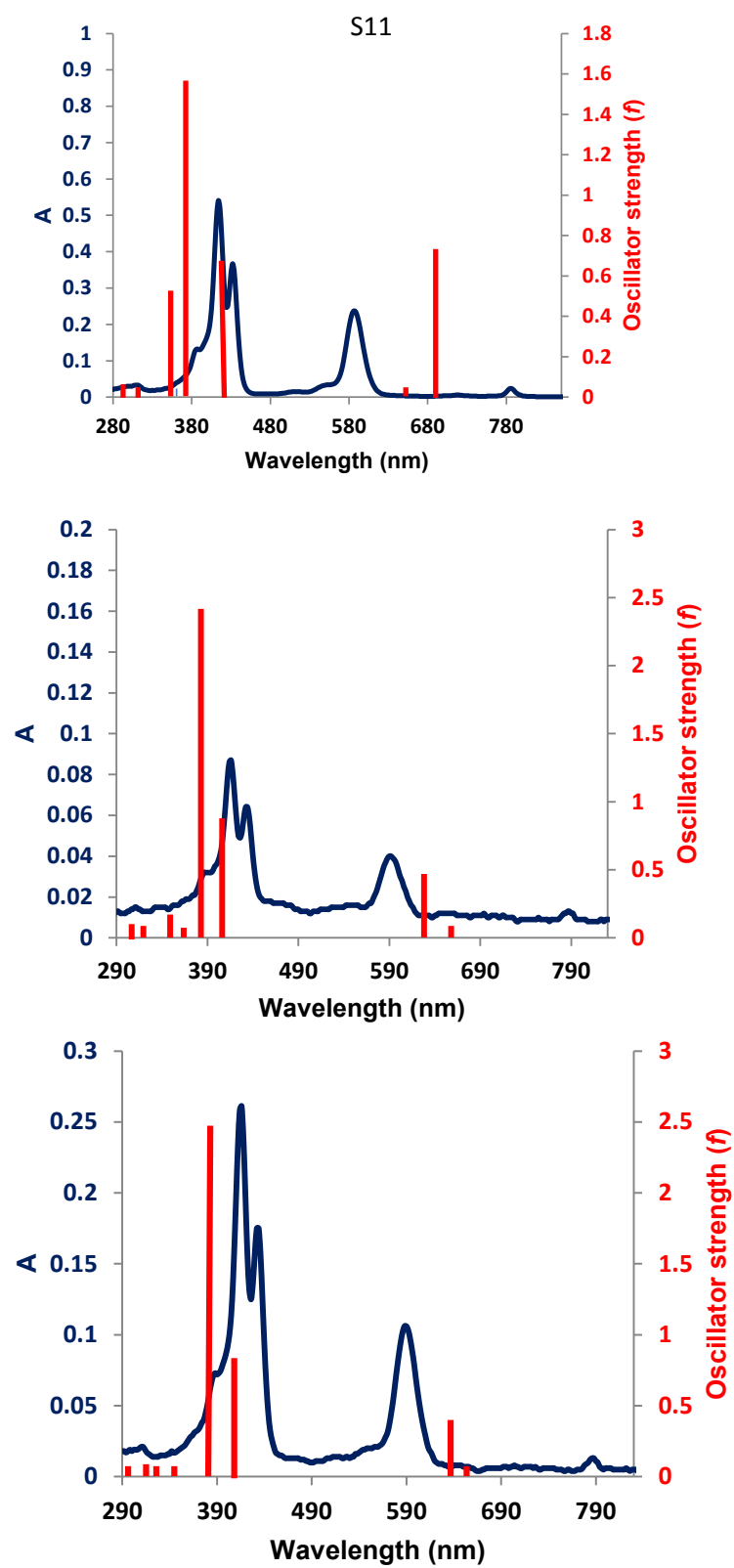


**Figure S13:** The steady state absorption spectra (blue line) of compounds **4-6** recorded in DCM along with the theoretical vertical excitation energies (red bar) obtained from TD-DFT calculations carried out at the B3LYP/6-311G basis set

S12

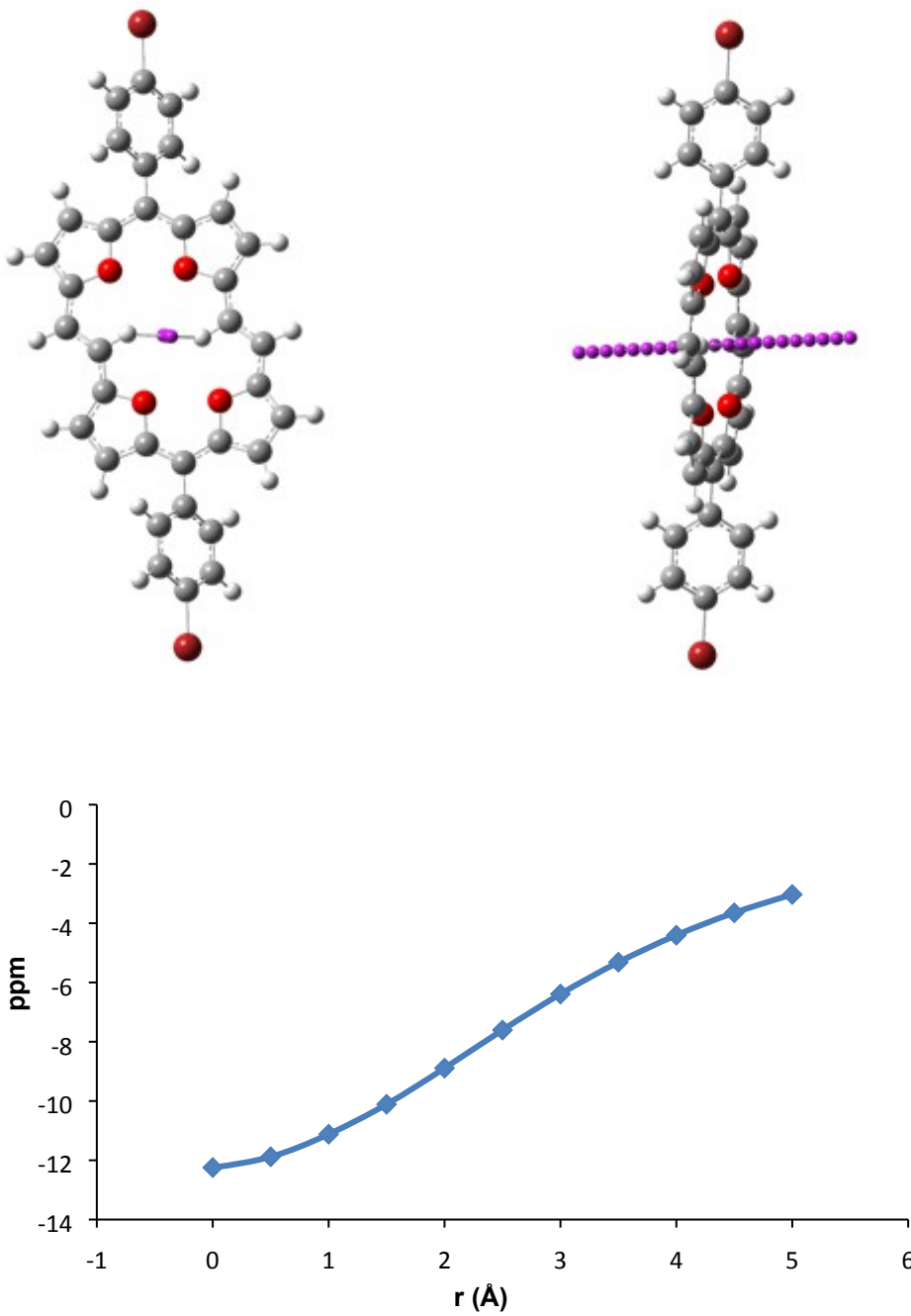


**Figure S14:** The ghost (Bq) atoms were placed at the centre of the molecule (in purple) at successive distances of  $0.5\text{\AA}$  to probe the aromaticity. The negative NICS values clearly display the aromaticity of **5**. At centre NICS is maximum and it goes on decreasing as we move farther from the centre.

S13

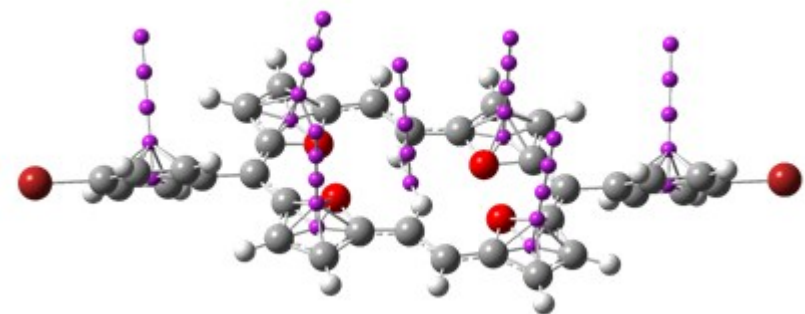
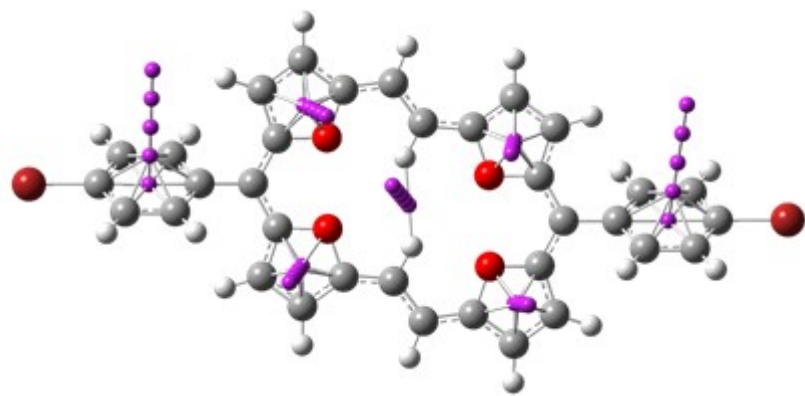
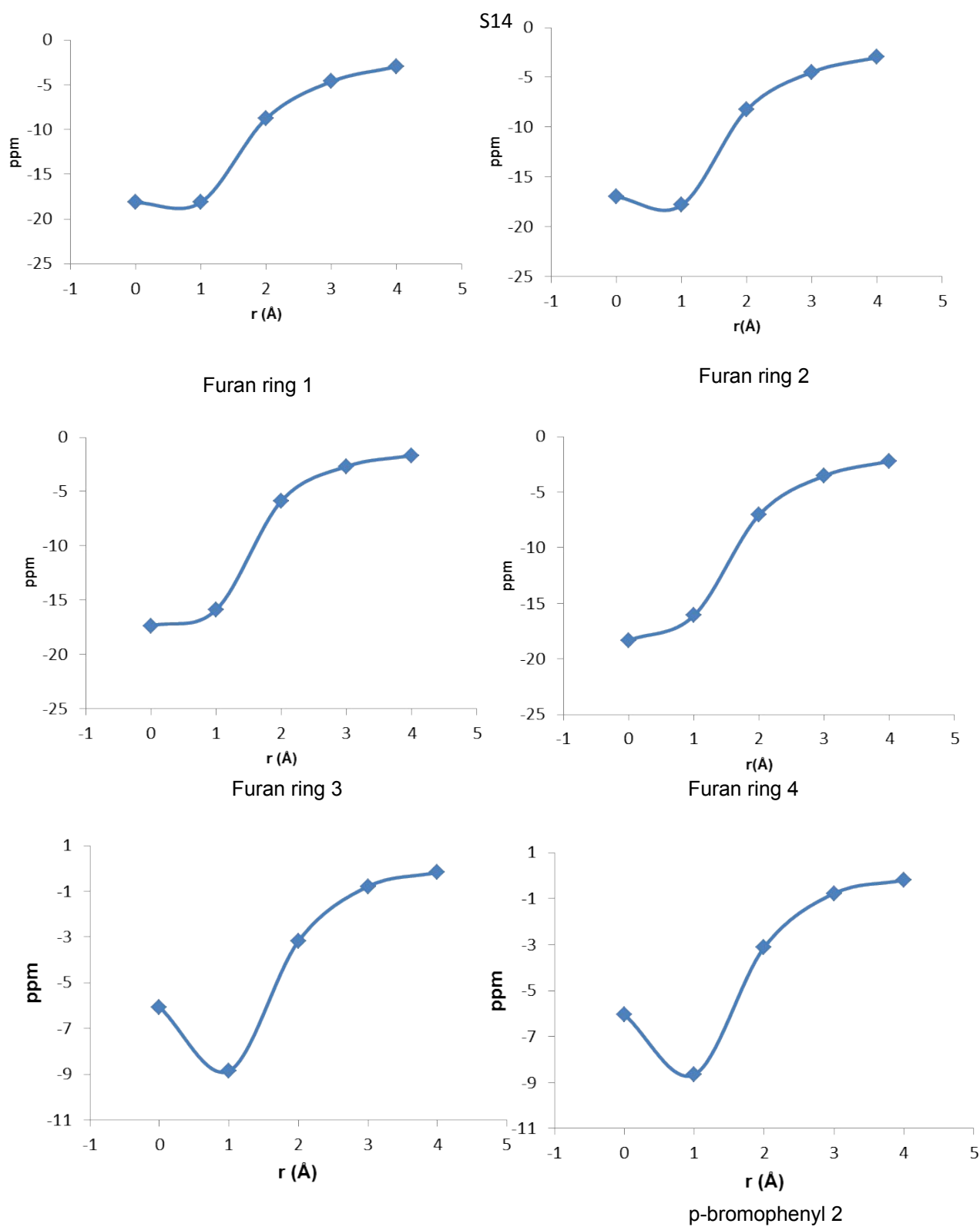


**Figure S15:** Calculation of NICS values for all individual rings in **5**. The calculation was performed by placing ghost atoms at 1 Å interval. The NICS vs r (distance from center) graphs are shown on next page.



p-bromophenyl 1

**Figure S16:** As shown above a set of two furan rings of **5** (attached to one of the trans double bond) are showing a dip at 1Å in the calculated NICS values. The behaviour of two furan rings is also different from an isolated furan ring (which shows no dip at 1Å). p-Bromophenyl rings are showing normal behaviour as bromobenzene but with decreased NICS values.

S15

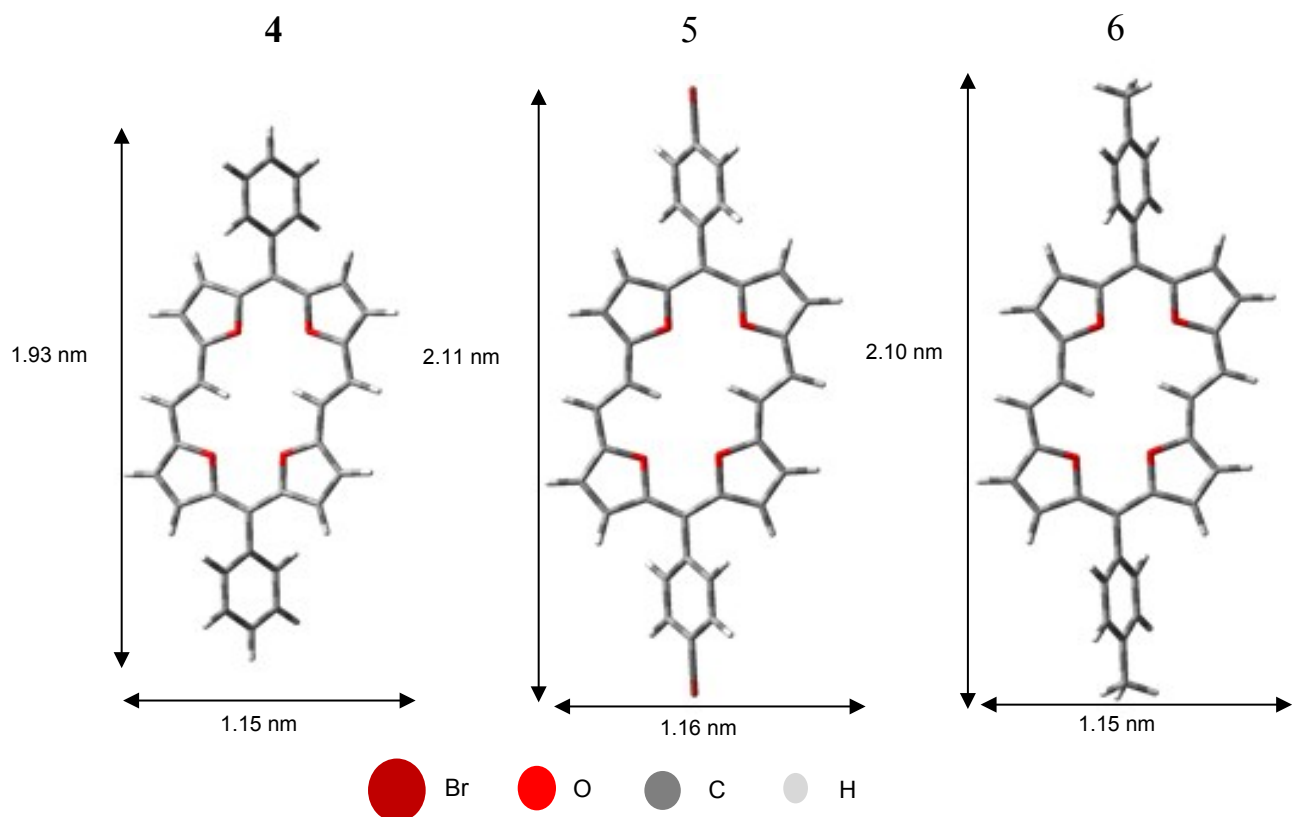


**Figure S17:** Molecular structures (optimized at Gaussian 09 B3LYP/6-311G (d)) and their molecular dimensions.

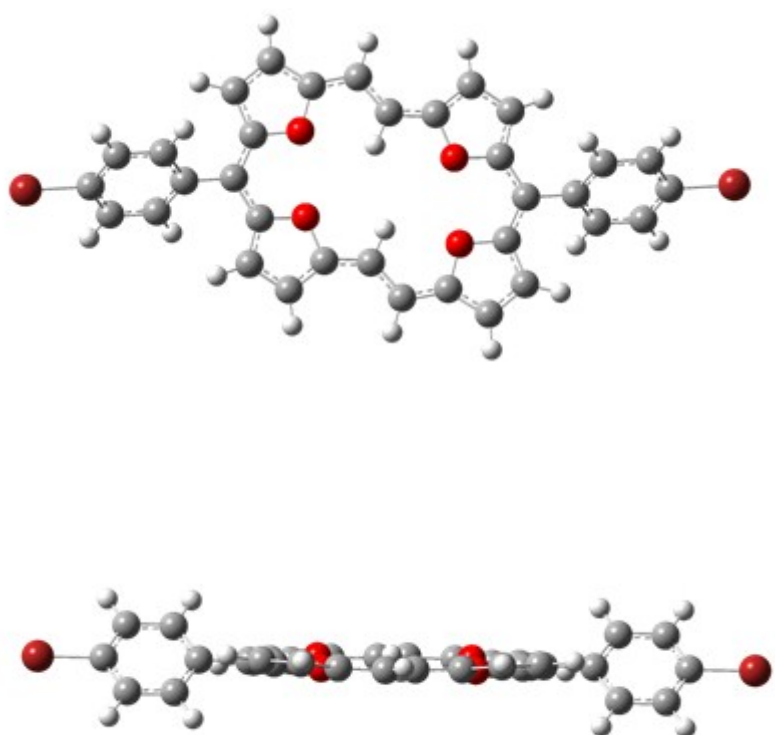


**Figure S18:** Energy minimized structure of **5** by DFT method at B3LYP/6-311G(d) level using the Gaussian09 program (Top and side view).

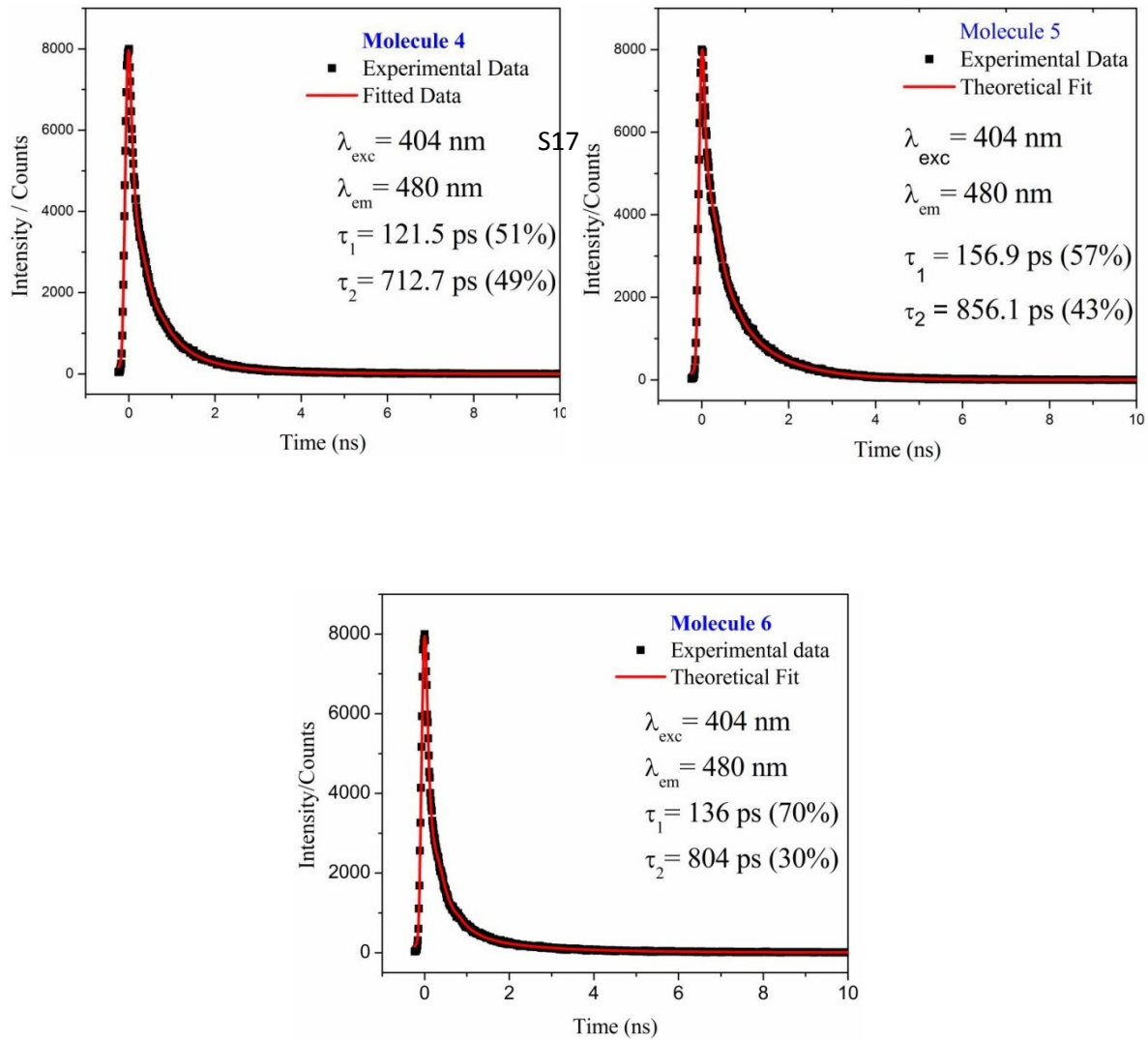


**Figure S19:** Fluorescence lifetimes of three compounds measured through TCSPC with IRF of 80 ps.

**Table S1:** Selected TD-DFT ( B3LYP/6-311G (d)) calculated energies, oscillator strengths and compositions of the major electronic transitions of **4**

<b>Energy (cm<sup>-1</sup>)</b>	<b>λ (nm)</b>	<b>Osc. Strength(<i>f</i>)</b>	<b>Major contributions</b>
14478.45	690.68	0.7216	HOMO → LUMO (92%)
15307.59	653.27	0.0199	H-1 → LUMO (52%), HOMO → L+1(46%)
23748.98	421.06	0.6697	H-1 → LUMO (49%), HOMO → L+1 (54%)
24192.59	413.34	0	HOMO → L+2 (81%)
26740.49	373.97	1.5637	H-1 → L+1 (53%), HOMO → L+3 (40%)
27997.91	357.17	0	HOMO → L+4 (97%)
28010.81	357	0.0026	HOMO → L+5 (98%)
28176.96	354.90	0	H-2 → LUMO (76%)
28268.91	353.75	0.5247	HOMO → L+3 (52%), H-1 → L+1 (29%)
29169.83	342.82	0	HOMO → L+6 (93%)
29447.29	339.59	0	H-3 → LUMO (82%)
30199	331.14	0	H-1 → L+2 (83%)
32175.05	310.80	0.0101	H-4 → LUMO (84%)
32564.62	307.08	0.0030	H-5 → LUMO (98%)
32633.18	306.43	0	H-6 → LUMO (97%)

**Table S2:** Selected TD-DFT ( B3LYP/6-311G (d)) calculated energies, oscillator strengths and compositions of the major electronic transitions of **5**

<b>Energy (cm<sup>-1</sup>)</b>	<b>λ(nm)</b>	<b>Osc. Strength (<i>f</i>)</b>	<b>Major Contributions</b>
15244	656	0.0217	H-1 → LUMO (56%), HOMO → L+1 (21%)
15967.35	626.29	0.4615	HOMO → LUMO (80%)
24752.34	404	0.8751	HOMO → L+1 (55%), H-1 → LUMO (42%)
26103.31	383.09	2.4108	H-1 → L+1 (64%), HOMO → LUMO (17%)
26236.40	381.15	0	HOMO → L+2 (82%)
28456.84	351.41	0	HOMO → L+4 (99%)
28480.23	351.12	0.0059	HOMO → L+5 (99%)
28589.92	349.78	0.1451	HOMO → L+3 (81%)
28901.25	346	0	H-2 → LUMO (60%), HOMO → L+6 (25%)
29531.17	338.63	0	H-1 → L+2 (90%)
29976.39	333.60	0	HOMO → L+6 (67%), H-2 → LUMO (19%)
31072.49	321.83	0	HOMO → L+7 (62%), H-4 → LUMO (29%)
31137.82	321.16	0.0011	HOMO → L+8 (99%)

31203.96	320.47	0	H-4 → LUMO (48%), HOMO → L+7 (37%)
31529	317.17	0.0536	H-1 → L+3 (78%), H-3 → LUMO (14%)

---

**Table S3:** Selected TD-DFT ( B3LYP/6-311G(d)) calculated energies, oscillator strengths and compositions of the major electronic transitions of **6**

Energy (cm <sup>-1</sup> )	λ (nm)	Osc. Strength ( <i>f</i> )	Major Contributions
15340.66	651.87	0.0170	H-1 → LUMO (56%), HOMO → L+1 (44%)
15760.07	634.53	0.3985	HOMO → LUMO (80%)
24591.03	406.65	0.8277	HOMO → L+1 (55%), H-1 → LUMO (44%)
26163	382.22	2.4631	H-1 → L+1 (70%), HOMO → LUMO (20%)
26521.92	377.04	0	HOMO → L+2 (80%)
29067.4	344.02	0.0321	HOMO → L+3 (91%)
29098.05	343.67	0	H-2 → LUMO (56%), HOMO → L+4 (27%)
29478.74	339.23	0	HOMO → L+4 (70%), H-2 → LUMO (18%)
29805.4	335.51	0	H-1 → L+2 (85%)
29807.82	335.48	0.0014	HOMO → L+5 (94%)
30101.40	332.21	0	HOMO → L+6 (95%)
30982.16	322.77	0	H-3 → LUMO (75%), H-2 → L+1 (13%)
31862.92	313.85	0.0324	H-4 → LUMO (80%), H-1 → L+3 (9%)
32289.58	309.70	0.0116	H-1 → L+3 (88%)
32704.15	305.77	0	H-1 → L+4 (92%)

---

**Table S4:** Coordinates for the optimized structure **5**.

Center Number	Atomic Number	Atomic Type	Coordinates (Å)		
			X	Y	Z
1	8	0	-2.378445	1.623352	0.028894
2	8	0	-2.190042	-0.906875	-0.099126
3	6	0	-2.028418	2.975770	-0.101987
4	6	0	-3.222887	3.699798	-0.258254
5	1	0	-3.291152	4.766137	-0.387957
6	6	0	-4.289973	2.796875	-0.242478
7	1	0	-5.330527	3.036810	-0.366590
8	6	0	-3.769187	1.494228	-0.069203
9	6	0	-4.342693	0.210996	-0.022855
10	6	0	-3.580191	-0.972215	0.015036
11	6	0	-3.915637	-2.335953	0.192815
12	1	0	-4.912539	-2.715187	0.328647
13	6	0	-2.738883	-3.085453	0.193320
14	1	0	-2.664585	-4.151520	0.321740
15	6	0	-1.652868	-2.207686	0.021880
16	6	0	-0.258688	-2.228009	-0.018565
17	1	0	0.170876	-1.241241	-0.133273
18	6	0	0.654226	-3.263912	0.096095
19	1	0	0.351250	-4.297052	0.207645
20	6	0	-5.828758	0.098366	-0.013707
21	6	0	-6.598877	0.767268	0.954661
22	1	0	-6.103892	1.355420	1.714828
23	6	0	-7.990980	0.664376	0.967458
24	1	0	-8.569199	1.176455	1.722015
25	6	0	-8.625306	-0.116942	0.006049
26	6	0	-7.892603	-0.792088	-0.965723
27	1	0	-8.396134	-1.387559	-1.712579
28	6	0	-6.501184	-0.680153	-0.972862
29	1	0	-5.932911	-1.185688	-1.741114
30	8	0	2.378444	-1.623352	-0.028894
31	8	0	2.190042	0.906875	0.099125
32	6	0	2.028417	-2.975770	0.101989

33	6	0	3.222886	-3.699797	0.258259
34	1	0	3.291150	-4.766137	0.387962
35	6	0	4.289972	-2.796875	0.242483
36	1	0	5.330526	-3.036811	0.366596
37	6	0	3.769187	-1.494228	0.069205
38	6	0	4.342694	-0.210996	0.022855
39	6	0	3.580191	0.972216	-0.015039
40	6	0	3.915636	2.335953	S21192819
41	1	0	4.912539	2.715188	-0.328653
42	6	0	2.738883	3.085454	-0.193324
43	1	0	2.664585	4.151520	-0.321745
44	6	0	1.652868	2.207687	-0.021882
45	6	0	0.258688	2.228010	0.018564
46	1	0	-0.170876	1.241242	0.133273
47	6	0	-0.654227	3.263913	-0.096094
48	1	0	-0.351251	4.297052	-0.207644
49	6	0	5.828758	-0.098366	0.013707
50	6	0	6.598878	-0.767271	-0.954658
51	1	0	6.103893	-1.355426	-1.714824
52	6	0	7.990980	-0.664379	-0.967456
53	1	0	8.569200	-1.176461	-1.722011
54	6	0	8.625306	0.116942	-0.006049
55	6	0	7.892603	0.792091	0.965721
56	1	0	8.396135	1.387565	1.712575
57	6	0	6.501184	0.680157	0.972860
58	1	0	5.932911	1.185694	1.741110
59	35	0	10.573352	0.268808	-0.021460
60	35	0	-10.573352	-0.268809	0.021460

---

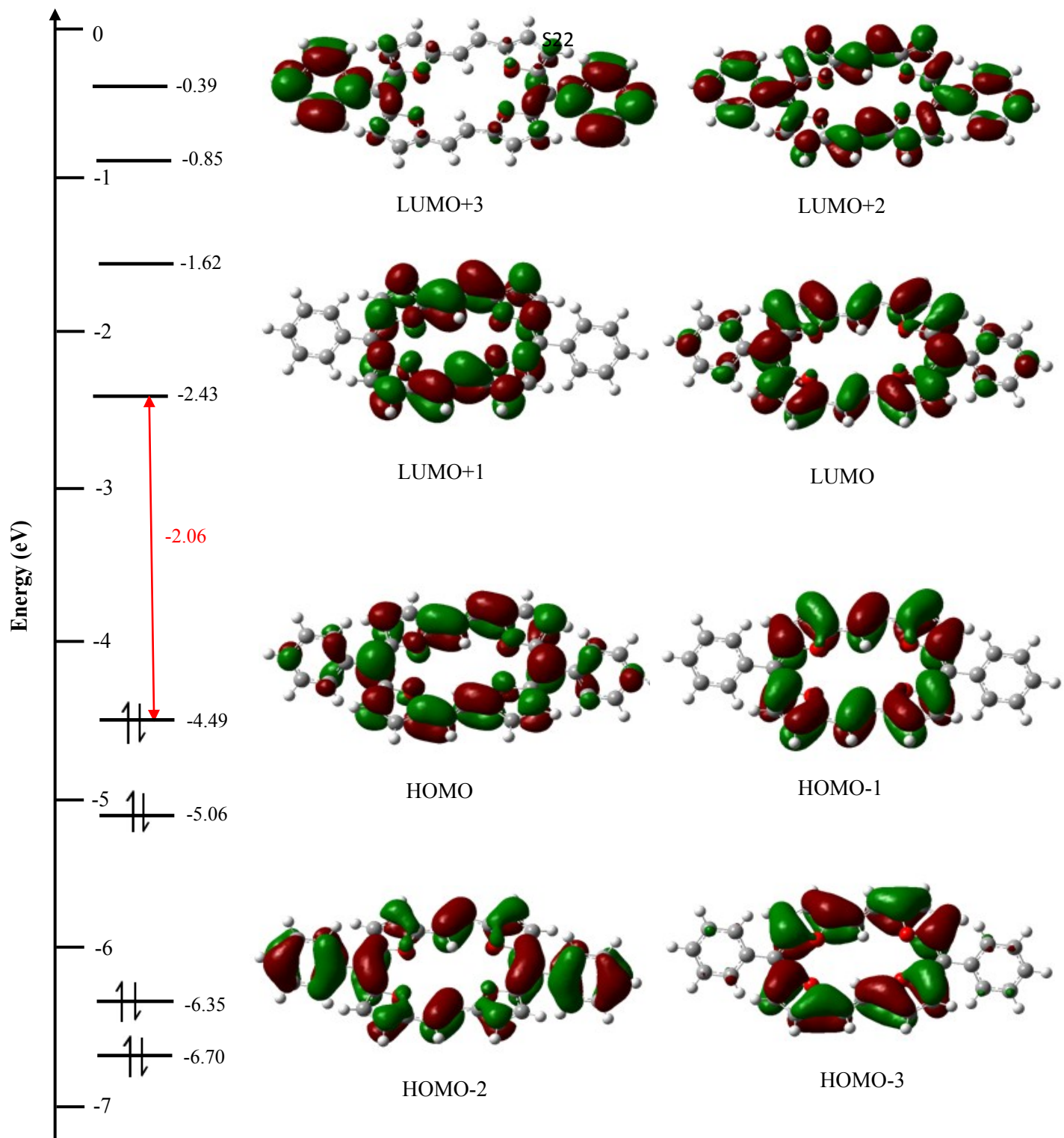


**Figure S20:** Selected Frontier MOs of **4** calculated at the B3LYP/6-311G(d) level.

S23

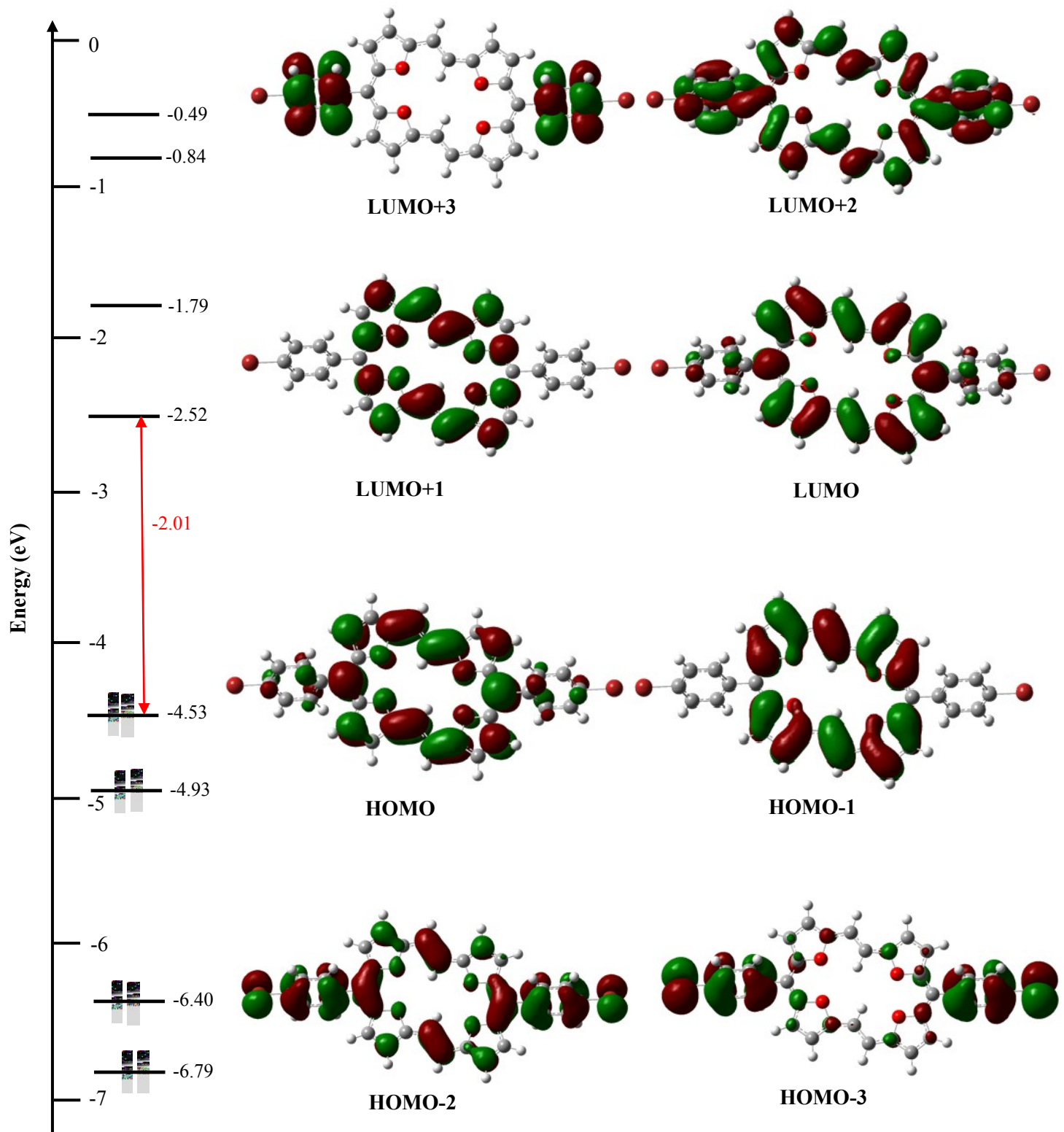


**Figure S21:** Selected Frontier MOs of **5** calculated at the B3LYP/6-311G(d) level.

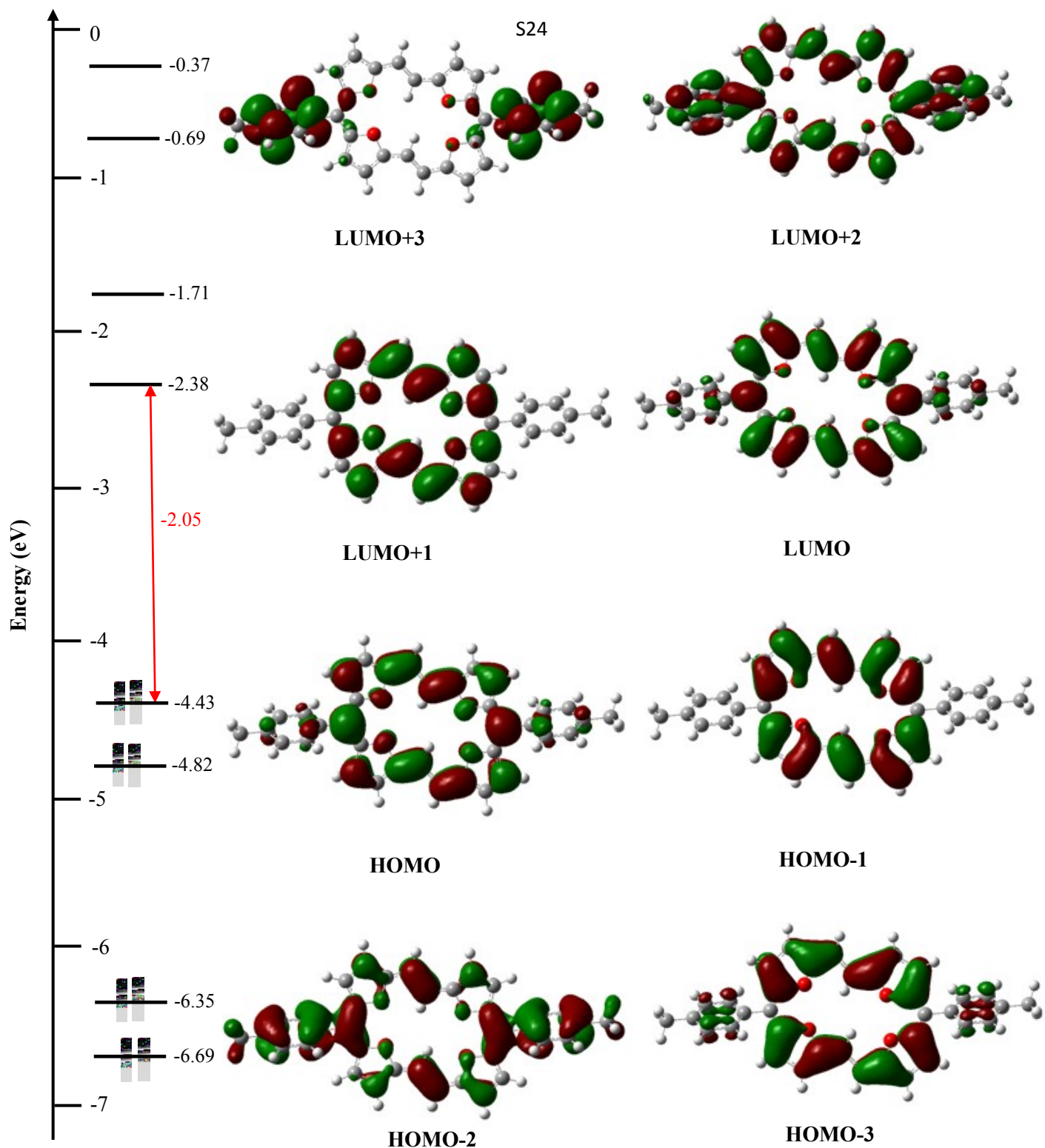


**Figure S22:** Selected Frontier MOs of **6** calculated at the B3LYP/6-311G (d) level.

S25

**Table S5:** Average polarizability ( $\alpha$ ) value calculated using Gaussian 09 program (keyword = polar).

	$\alpha_{xx}$	$\alpha_{xy}$	$\alpha_{yy}$	$\alpha_{xz}$	$\alpha_{yz}$	$\alpha_{zz}$	$\alpha \times 10^{-41}$ (Cm <sup>2</sup> V <sup>-1</sup> )
<b>4</b>	1328.581	12.809	522.212	0.377	7.417	189.812	1121.49
<b>5</b>	1233.367	-27.081	544.487	-1.528	-10.244	217.240	1141.10
<b>6</b>	1321.528	-37.929	542.123	-1.590	-10.988	212.627	1096.48

Polarizability,  $\alpha = 1/3 (\alpha_{xx} + \alpha_{yy} + \alpha_{zz})$ ; 1 au = 8.6396 X 10<sup>-33</sup> esu = 1.6487773 x 10<sup>-41</sup> Cm<sup>2</sup>V<sup>-1</sup>.

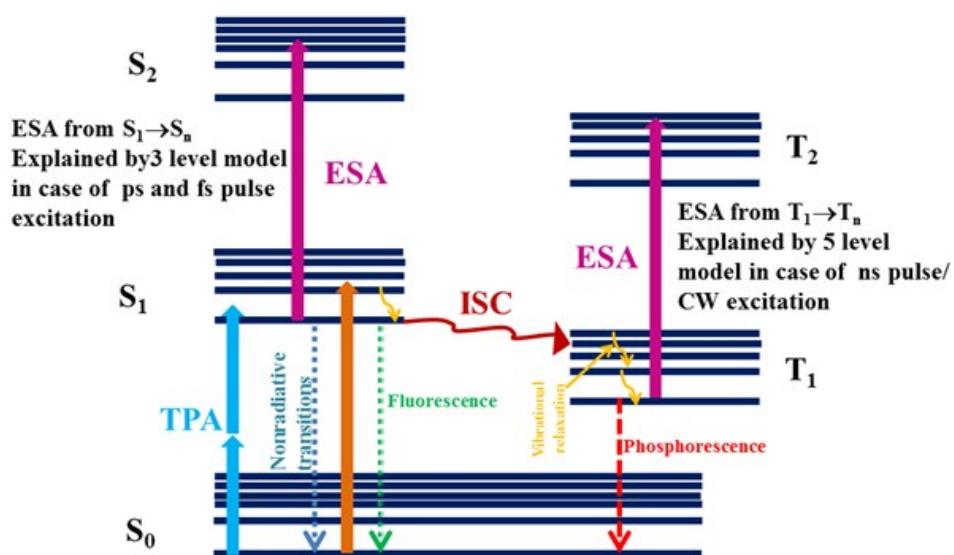


**Figure S23:** Five level energy state diagram to explain ESA assisted RSA in case of ns excitation which reduces to 3 level energy state diagram under ps and fs pulse excitations with practically no triplet states involved and only singlet state contributing.

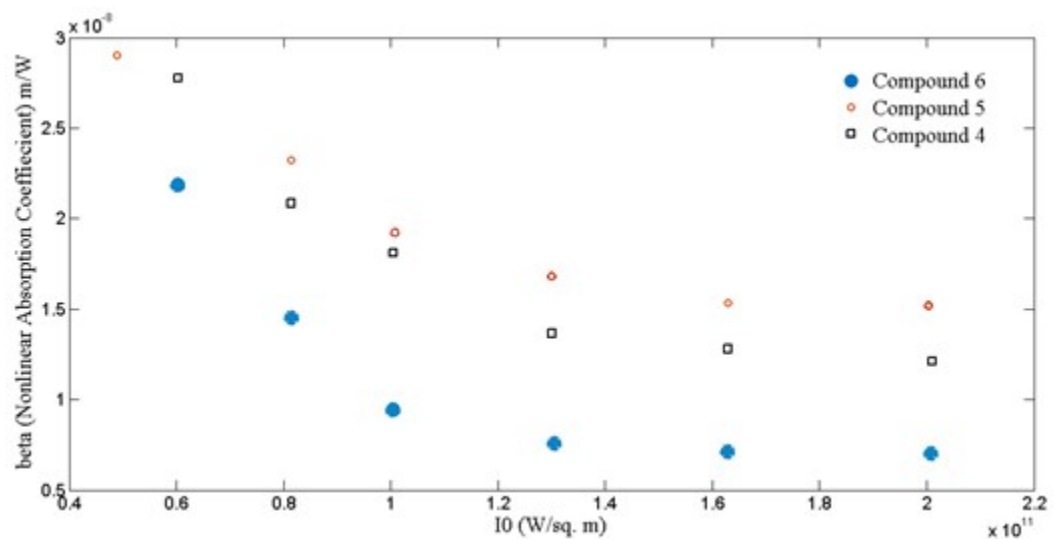


**Figure S24:** Plot of  $\beta$  versus on axis fluence  $I_0$  as a proof of ESA assisted RSA & not TPA

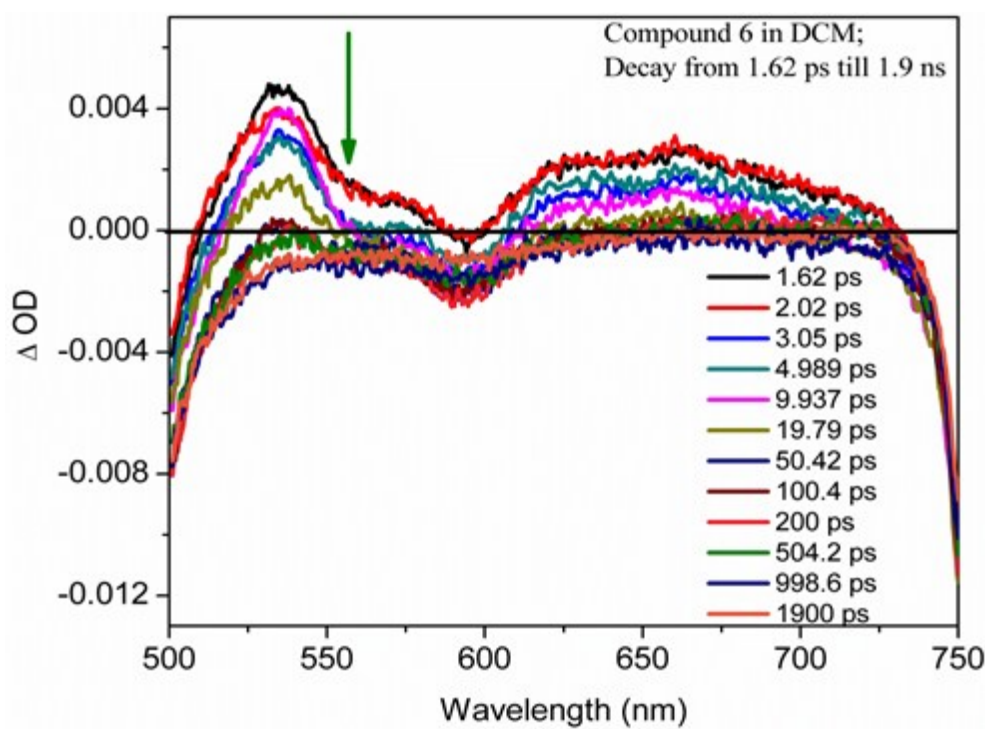
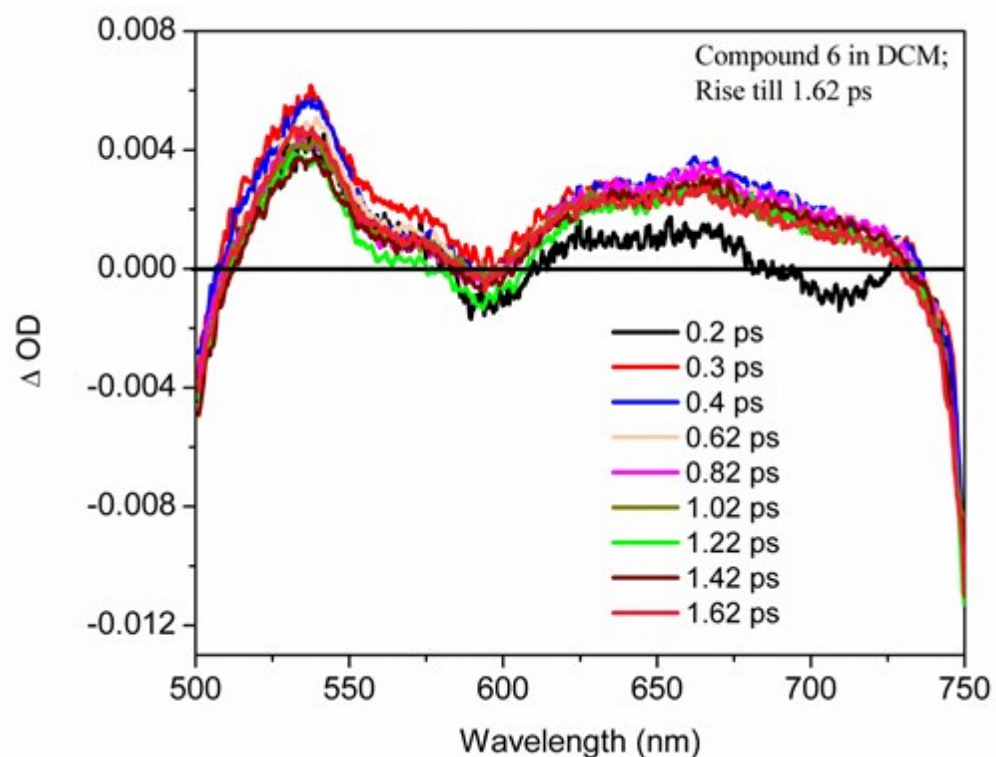


**Figure S25:** Femtosecond transient absorption spectra of compound **6** in DCM.

**Complete reference 17**

S29

M. J. Frisch, G. W. Trucks, H. B. Schlegel, G. E. Scuseria, M. A. Robb, J. R. Cheeseman, G. Scalmani, V. Barone, B. Mennucci, G. A. Petersson, H. Nakatsuji, M. Caricato, X. Li, H. P. Hratchian, A. F. Izmaylov, J. Bloino, G. Zheng, J. L. Sonnenberg, M. Hada, M. Ehara, K. Toyota, R. Fukuda, J. Hasegawa, M. Ishida, T. Nakajima, Y. Honda, O. Kitao, H. Nakai, T. Vreven, J. A. Montgomery, Jr, J. E. Peralta, F. Ogliaro, M. Bearpark, J. J. Heyd, E. Brothers, K. N. Kudin, V. N. Staroverov, R. Kobayashi, J. Normand, K. Raghavachari, A. Rendell, J. C. Burant, S. S. Iyengar, J. Tomasi, M. Cossi, N. Rega, J. M. Millam, M. Klene, J. E. Knox, J. B. Cross, V. Bakken, C. Adamo, J. Jaramillo, R. Gomperts, R. E. Stratmann, O. Yazyev, A. J. Austin, R. Cammi, C. Pomelli, J. W. Ochterski, R. L. Martin, K. Morokuma, V. G. Zakrzewski, G. A. Voth, P. Salvador, J. J. Dannenberg, S. Dapprich, A. D. Daniels, O. Farkas, J. B. Foresman, J. V. Ortiz, J. Cioslowski and D. J. Fox, Gaussian 09, Revision A.02, Gaussian, Inc., Wallingford CT, **2009**.

S30